Ocean Engineering 272 (2023) 113859

Contents lists available at ScienceDirect

Ocean Engineering

journal homepage: www.elsevier.com/locate/oceaneng

A simplified approach for fatigue life prediction of aquaculture nets under waves and currents

Martin Slagstad *, Zhaolong Yu, Jørgen Amdahl

Centre of Autonomous Marine Operations and Systems, Department of Marine Technology, Norwegian University of Science and Technology, NTNU NO-7491 Trondheim, Norway

ARTICLE INFO

Keywords:
Force response
Aquaculture net
Analytical
Simplified method

ABSTRACT

With increasing trends to move fish farms to more exposed locations engineers need quick and accurate tools for creating initial design proposals. In this paper, a simplified analytical model for estimating the axial force in the ropes supporting the fish net is presented. Hydrodynamic loads acting on the net are calculated using a state of the art screen model. The simplified analytical model is a quasi-static solution based on the principle of virtual displacements. The assumed mode shape in the calculations is a simplification of the actual quasi-static displacement shape under combined wave and current loading in view of the high natural frequencies of pre-tensioned ropes compared to wave frequencies. The results from the simplified calculations are compared to numerical simulations performed in RIFLEX. The simplified method is extremely efficient with regard to computation time compared to the numerical simulations and is well suited for preliminary design of fish nets.

1. Introduction

Farming of salmon is one of Norway's largest industries. As of 2019 the annual value of export was 75 billion NOK. In recent years, fish farms have become larger and they are being placed in more exposed locations. Moving to harsher environments will increase the importance of wave loads. In addition, the current velocities are expected to increase. Jusoh and Munshi (2018) presents a design current of 1.5 m/s in the southern north sea compared to 1.0 m/s at an exposed fish farm location, (Bore and Amdahl, 2017).

Currently, the design of fish nets and the supporting structure is mainly based on empirical methods, (Standards Norway, 2009). These methods may not be accurate when the environment changes drastically by moving to harsher areas. For these novel cases, methods based on physical considerations are needed to ensure that the confinement system is sufficiently robust to avoid failure and prevent fish from escaping.

Structural failure is pointed out to be the largest contributor to fish escape, (Jensen et al., 2010). Structural failure is not an event that has occurred frequently, but is related to a large number of escaped fish for each event. Failure of aquaculture nets is by far the dominating means of reported escape, (Jensen et al., 2010).

There are in general, two different methods that may be used to estimate the viscous forces on fish nets, namely Morrison type models and screen type models, (Bore et al., 2017). The Morrison type of model has either constant coefficients or coefficients depending on Reynolds number (Re) and the net's solidity ratio (Sn). See for example Faltinsen and Timokha (2009). The Reynolds number is calculated based on the twine diameter and the solidity ratio is defined as projected area of the net in the normal direction divided by the total area spanned by the panel. Screen models such as, Loland (1991) and Kristiansen and Faltinsen (2012) depend additionally on the angle of the flow. Thus, screen type models have the advantage that they estimate the force more accurately when the flow has an angle compared to the normal of the net. A challenge is however that the screen models are not available in many commercial software. Recently, model tests in uniform current were performed by Moe Føre et al. (2020) and Moe-Føre et al. (2021) to further improve the accuracy of the force estimation on fish nets.

Lader et al. (2007) and Dong et al. (2019) show that the normal forces acting on fish net panels in regular waves are well estimated using formulas based on constant flow. Zhao et al. (2008) shows from experimental results that the drag force acting on a fish net panel in waves is constant for Keulegan–Carpenter, (KC) numbers in the range 150–400 and Dong et al. (2019) indicates that the drag coefficient changes very little for a KC number above 50. Due to the large KC number in physical wave conditions, the flow may be assumed to be quasi-steady, (Kristiansen and Faltinsen, 2015). Force models developed for steady current conditions are therefore considered applicable also for oscillating current due to waves.

The forces acting on the net structure can be accurately calculated using non-linear finite element programs. Examples are presented for

* Corresponding author.
E-mail address: martin.slagstad@ntnu.no (M. Slagstad).

https://doi.org/10.1016/j.oceaneng.2023.113859
Received 16 November 2022; Received in revised form 17 January 2023; Accepted 31 January 2023
Available online 4 February 2023

Nomenclature

α	Location parameter for maximum displacement
$\bar{a}$	Fatigue constant for steel
$\bar{m}$	Mass per unit length
$\bar{w}$	Rope amplitude
$\Delta\sigma$	Stress range
δW_e	External virtual work
δW_i	Internal virtual work
ω	Wave frequency
ρ	Density of sea water
σ	Stress
ε	Strain
ζ	Wave amplitude
A	Cross section area
$a_t(T)$	Temperature dependency for creep model
C_N	Normal viscous force coefficient
C_T	Tangential viscous force coefficient
C_{strain}	Constant for creep model
d	Diameter
E	Young's Modulus
f_N	Viscous normal force
f_T	Viscous tangential force
K	Initial stiffness
k	Wave number
K_a	Axial Stiffness
L	Length
m	Slope of SN and creep curve
N	Number of cycles
R	Motion ratio
S	Tension in rope
S_0	Pretension in rope
S_N	Tension in rope from normal loading
S_T	Tension in rope from tangential loading
Sn	Solidity ratio
T	Temperature
T_0	Natural period
u_c	current velocity
u_w	wave particle velocity
u_{rel}	Relative velocity
u_{rope}	Rope velocity
u_{w_a}	wave particle velocity amplitude
w	Rope displacement
z_b	Bottom coordinate of rope
z_t	Top coordinate of rope

pure current conditions in Moe-Føre et al. (2016) and Mjåtveit et al. (2021) and for both current and waves in Kristiansen and Faltinsen (2015). Mohapatra et al. (2021) presents results from numerical and analytical analysis of flexible net cages. The accuracy of the results using NLFEA is usually high but the computation time is large, which may be acceptable for design verification. In early design stages it is however, desirable to have simpler and faster methods, with a reasonable accuracy.

In the present paper a simplified method to calculate the force response in the vertical ropes supporting aquaculture nets is proposed and compared to numerical simulations. The estimated fatigue life of the rope is used as the main comparison parameter to investigate the accuracy of the simplified method. The main contribution of the current paper is to present a rational method for fast and reliable assessment of the force response in the ropes supporting the aquaculture nets. The objectives of developing the simplified method are twofold; 1. It can be used in the design phase, 2. To check the results of complex analyses such as NLFEA. This is not yet a formal requirement for aquaculture structures. It may therefore be useful to consider requirements in other industries. For example, for oil and gas installations on the Norwegian Continental shelf the NORSOK standard N-001 concerning "Integrity of Offshore Structures" specifies among others in Section 5.3 "General requirements relating to personnel qualifications, quality assurance and organization": "structural engineers qualify their own analysis by self checking using simplified models and by alternative calculations of relevant structural part where faults can entail major consequences. Documentation for these simplified calculations shall be available". In addition, the simplified method gives a good overview of the contribution from different hydrodynamic effects acting on the moving net and thereby increases our knowledge of the response.

Fig. 1. Ocean farm 1 at inspection draft.

The simplified method is a closed form solution and will generally be quicker than a NLFEA solution where the equation of motion must be solved. For problems such as fish nets, NLFEAs generally require a very small time step to be stable and have therefore a rather large computation time. For the simple method there is no time step limitation.

2. Description of the problem

Inspired by novel offshore farm designs such as the Ocean Farm 1 shown in Fig. 1, we consider a plane net panel connected to a rigid frame as shown in Fig. 2. Only waves propagating perpendicularly to the net panel are considered in the present paper.

Structurally, the net's load bearing system is constructed similar to a stiffened panel. The net itself is supported by a number of vertical ropes with even spacing. The ropes have generally a larger stiffness than the net itself, see Section 2.1. In addition, the ropes are under pretension which further increases the initial stiffness. A hypothesis is therefore postulated that it is possible to estimate the response of the net similar to that of a stiffened panel by only considering a single rope/(one stiffener with plate flange) rather than accounting for the whole panel. The problem is then simplified to solve for the rope response under the action of the hydrodynamic loads on the rope itself and that transferred from the net, (ref. Fig. 2). The validity of considering the response of a single rope to represent the response of a panel is verified and discussed using numerical simulations in Section 5.1.

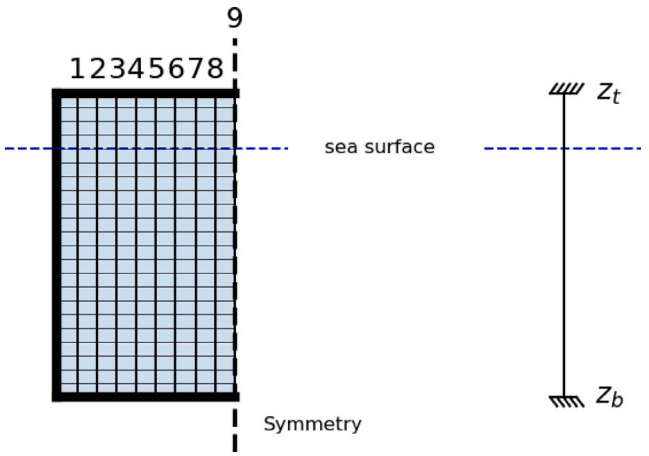

Fig. 2. To the left, Half of the analysis model of a complete panel. Vertical ropes are shown with numbers. Fish net elements with thin horizontal black lines. Thick black lines are beams supporting the net panel. The shaded area represents the net. To the right; Simplified model of one rope used in the analyses in the present paper. Model is clamped at both ends.

Table 1
Properties of the fish net and supporting rope.

	Rope	Net
Diameter, D [mm]	30	1.84
E-modulus, E $\frac{N}{mm^2}$	7.96e10	1.62e9
Spacing/Halfmesh, L [mm]	1650	23.3
mass $\frac{kg}{m}$, $\frac{kg}{m^2}$	0.71	0.59

2.1. Net properties

The net and rope properties are shown in Table 1. The pretension acting on the rope is 100 kN.

The axial stiffness of the rope and net per unit width, K_a is calculated using the following equation:

$$K_a = \frac{\pi E d^2}{4L} \tag{1}$$

For the net, the stiffness is 1.8e5 N/m and for the rope, the stiffness is 3.4e7 N/m. The net is hence approximately 100 times softer than rope.

3. Fatigue failure

The authors are not able to identify any published work on fatigue of aqua culture nets or the supporting structure (the vertical ropes) other than in Wang et al. (2020) where results from material tests for copper nets are presented. The reason for the lack of work is likely to be three-fold; 1. environmental loads have been limited since traditional sites are generally rather sheltered. 2. "Dimensioning of net pens has traditionally been empirical design" (Standards Norway, 2009). 3. the fish nets are often taken on shore after every production cycle for disinfection at a service station, (Føre et al., 2019). According to Soares et al. (2011) a production cycle varies between 54 and 124 weeks. If necessary, the nets can be recertified or replaced while they are on shore.

When moving to larger structures and to more exposed areas, it is desirable to avoid disassembling the net between production cycles. One such structure is the Ocean Farm 1 where the net is disinfected on site by raising the platform to the inspection draft. With increasing dynamic loads from the increased wave heights and current velocities and a more challenging inspection/certification process, it is reasonable to require that the capacity of the nets be better documented than before.

Calculation methods for fatigue failure of ropes are not as well established as for steel. The models that exist for estimating the fatigue life depend on the material of the rope. The OF1 ropes used to support the net are made from a material called *Dyneema* DM20. There is strong evidence that the failure of such ropes is dominated by creep failure rather than failure due to cyclic loading, (Vlasblom et al., 2017, 2019) and DSM (2008).

The fatigue life of the OF1 ropes can be estimated using creep calculations. Humeau et al. (2018) presents a model for estimating the lifetime expectany for tension fatigue of HMPE-ropes (High Modulus PolyEthylene). The dynamic strain ε as a function of time, t, can be calculated according to:

$$\varepsilon = \int_0^t \dot{\varepsilon}_{pl-d}\, dt \tag{2}$$

Once the plastic strain reaches a critical value, $\varepsilon_{pl-crit}$, the rope will fail. The dynamic plastic strain rate, $\dot{\varepsilon}_{pl-d}$, as a function of stress σ and temperature, T can be calculated using Eq. (3).

$$\dot{\varepsilon}_{pl-d}(\sigma, T) = C_{strain} a_t(T)\, \sigma^m \tag{3}$$

The parameters needed for the creep calculations are however trade secretes and are therefore not available for public use. Consequently, Eq. (3) is simplified in the present paper by,

$$\dot{\varepsilon}_{pl-d}(S) = C^*_{strain} S^m \tag{4}$$

S is the axial force in the rope.

Without access to proper constants the actual fatigue damage cannot be calculated. The results can however be normalized and compared to each other. Based on Humeau et al. (2018) using $m = 4.0$ and $\varepsilon_{pl-crit} = 0.26$ seems reasonable. The value of C^*_{strain} will not affect how different loads contribute since it is only a constant and will disappear during normalization.

In addition to calculating the fatigue life of the rope, the fatigue damage for the connection point of the rope, which is a steel structure, is calculated based on methods in DNV (2014). The damage estimates are based on the stress amplitudes and a single slope SN-curve. The stress in the steel detail is estimated using an assumed stress concentration factor between the axial force in the rope and the stress in the steel detail. The accumulated damage, D, is calculated using the Miner summation for the axial force range, ΔS,

$$D = \frac{1}{\bar{a}} N (\Delta S)^m \tag{5}$$

m = 3.0 and $\bar{a}$ = *arbitrary constant* are used in the calculations for the steel connection. N is the number of cycles. The value of $\bar{a}$ is not very important since the results are normalized similar to that of the rope.

There is a significant difference between the two fatigue calculation methods presented above. Creep-fatigue, ref. Eq. (4), is dependent on the total force while the cyclic fatigue, ref. Eq. (5), is dependent on the change in force, i.e. the force amplitude. The rope could therefore fail due to creep-fatigue without dynamic loading whereas without dynamic loading damage to the steel connection will not occur.

4. Simple quasi-static response estimation of axial force in rope

The dynamic response of structures can generally be split into 3 domains: 1. inertia domain, 2. dynamic domain and 3. stiffness domain. Due to the low mass and large stiffness of the supporting ropes, the natural period is low. The response is therefore in the stiffness domain and can be calculated quasi-statically. This assumption is verified and discussed in Section 4.6.1.

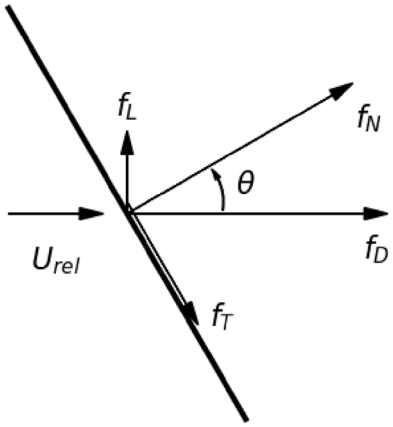

Fig. 3. The force components;drag f_D, lift f_L, normal component f_N and tangential component f_T.

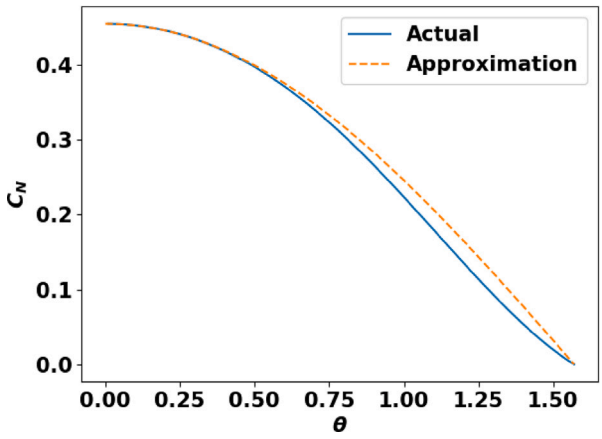

Fig. 4. Approximation of C_N according to Eq. (10).

4.1. Viscous forces acting on the fish net

The load model used to calculate the viscous loads is a state of the art screen model. The specific model used in the analysis is the screen model proposed by Loland (1991). The main reason for choosing this model is that it is included in the numerical software RIFLEX (Ocean, 2020) which is used to generate numerical simulations. The force components acting on the net is illustrated in Fig. 3. The screen model proposed by Løland decomposes the total force to a drag component, f_D, and a lift component, f_L. The drag coefficient, C_d, and lift coefficient, C_l, are defined as:

$$C_d\left(Sn,\theta\right) = 0.04 + \underbrace{\left(-0.04 + 0.33Sn + 6.54Sn^2 - 4.88Sn^3\right)}_{C_{D_0}}\cos\left(\theta\right) \tag{6}$$

$$C_l\left(Sn,\theta\right) = \underbrace{\left(-0.55Sn + 2.3Sn^2 - 1.76Sn^3\right)}_{C_{L_0}}\sin\left(2\theta\right) \tag{7}$$

In the simplified model these components will be transformed to a normal force, f_N, and a tangential force, f_T using Eq. (8) to Eq. (10) which yields the following coefficients.

$$C_T = \frac{C_{D0}sin\left(\theta\right) - C_{L0}sin\left(2\theta\right)}{tan\left(\theta\right)sin\left(\theta\right) + \cos\left(\theta\right)} \tag{8}$$

between $0 < \theta < \frac{\pi}{2}$, and

$$C_N = \frac{C_{L_0}sin\left(2\theta\right) + \left(0.04 + C_{D_0}cos\left(\theta\right)\right)\frac{cos(\theta)}{sin(\theta)}}{sin\left(\theta\right) + \frac{cos(\theta)^2}{sin(\theta)}} \tag{9}$$

between $0 < \theta < \frac{\pi}{2}$, where C_{D_0} and C_{L_0} are defined in Eqs. (6) and (7) respectively.

The expression for C_N is simplified to

$$C_N \approx C_N\left(0\right)cos\left(\theta\right) = \left(0.04 + C_{D_0}\right)cos\left(\theta\right) \tag{10}$$

The error of the approximation of C_N is small as shown in Fig. 4.

The normal and tangential force components can be written:

$$f_N\left(z\right) = \frac{1}{2}\rho AC_N\left(\theta\right)U\left(z\right)\left|U\left(z\right)\right| \tag{11}$$

$$f_T\left(z\right) = \frac{1}{2}\rho AC_T\left(\theta\right)U\left(z\right)\left|U\left(z\right)\right| \tag{12}$$

where $U\left(z\right)$ is the magnitude of the combined current and wave particle velocities, ρ the density of the sea water and A the projected area of the net panel. In the present paper, the wave particle velocities are calculated assuming regular waves and deep water conditions.

4.2. Simple quasi-static response for tangential loading C_T

The axial force in the rope due to the action of the viscous tangential force, f_T, is calculated assuming that the rope is in its initial position, i.e. as a straight line. The tangential force is only balanced by the stiffness of the rope and thereby changing the axial force in the rope. Since the viscous load, f_T, is distributed vertically along the rope, the axial force in the rope will change as a function of the water depth. Here we consider only the axial force at the top connection where it reaches a maximum.

The axial force from the tangential force, f_T, at the top connection point is then found by solving Eq. (13) numerically.

$$S_T = \frac{1}{2}C_T\left(\theta\right)\rho A\omega^2\zeta_a^2\int_{z_b}^{\zeta}\frac{z - z_b}{L}e^{2kz}dz \tag{13}$$

when it is assumed that the rope force transferred to the top connection, s_T, from a point load, $f_T\left(z\right)$, is given by

$$s_T\left(z\right) = \frac{L - \bar{z}}{L}f_T\left(z\right) \tag{14}$$

where $\bar{z}$ is the distance from the end connection.

ω is the circular frequency of the wave and ζ_a is the wave amplitude. z_b is the z-coordinate at the bottom of the rope.

4.3. Quasi-static deformation modes of a rope in regular waves

Before the calculation method for the axial force in the rope due to the normal loading is shown, the analytical expression for the quasi static deformation of a rope due to the normal load in a regular wave is derived. The procedure can also be used to derive the shape for pure current or combined wave and current.

The change in angle due to the loading is equal to:

$$d\theta = \frac{-f_N\left(z\right)dz}{S} \tag{15}$$

where $f_N\left(z\right)$ is the normal force per unit length and S is the axial force. Introducing the force amplitude in regular waves as:

$$f_N\left(z\right) = \underbrace{\frac{1}{2}\rho AC_N}_{C}U^2 = C\omega^2\zeta^2e^{2kz} \tag{16}$$

the angle of the catenary, θ, is found:

$$\theta = \int\frac{-f_N\left(z\right)}{S}dz = -\frac{C\omega^2\zeta^2}{2kS}e^{2kz} + \frac{C\omega^2\zeta^2}{2kS} - \theta_{t0} \tag{17}$$

where C is defined in Eq. (16). when $\theta\left(0\right) = -\theta_{t0}$. The horizontal displacement, x is found from

$$\theta = \frac{dx}{dz} \rightarrow x = \int\theta dz \tag{18}$$

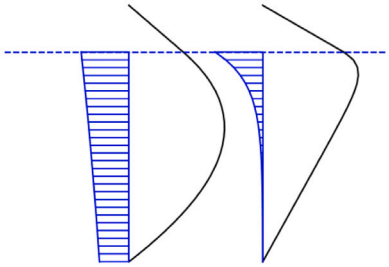

(a) Analytical deformation of net with constant tension for unit displacement. The dashed line is the waterline. Blue is velocity profile. Black is rope deformation. Left, T = 15 s. Right, T = 4 s

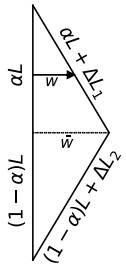

(b) Deformation mode for the principal of virtual displacements.

Fig. 5. Analytical and assumed deformation mode for quasi-static analysis.

Applying the boundary condition: $x(0) = x_0$ yields the following expression:

$$x = -\frac{C\omega^2\zeta^2}{4k^2S}e^{2kz} + \left(\frac{C\omega^2\zeta^2}{2kS} - \theta_{t0}\right)z + \frac{C\omega^2\zeta^2}{4k^2S} + x_0 \tag{19}$$

where

$$\theta_{t0} = \frac{F_{top}}{S} = -C\omega^2\zeta^2\frac{\frac{z_b}{2k}\left(1 - e^{2kz_b}\right) - \frac{1}{4k^2}\left(-1 - e^{2kz_b}\left(2kz_b - 1\right)\right)}{S\left(z_t - z_b\right)} \tag{20}$$

$$x_0 = \theta_{t0}z_t \tag{21}$$

The quasi-static deformation shapes for two different wave periods are shown in Fig. 5 together with the shape of the velocity profiles. Long periods yield a relatively uniform load, small periods yield a more concentrated load and the deformation pattern approaches a triangle.

4.4. Simple quasi-static estimation of axial force for normal loading, C_N

In this section a simplified model for estimating the axial force in ropes supporting the fish net due to the loads acting normally to the net is proposed. The derivation is based on the virtual work principle.

It is assumed that the net deforms in the triangular shape shown in Fig. 5(b). The displacement along the rope can then be written as $w(z) = \phi(z)\bar{w}$. The mode shape, $\phi(z)$, is a simplification of the complicated quasi-static solution shown in Fig. 5(a) and is of course best for small wave periods. The location of maximum deformation, αL matches the location based on the solution of the actual quasi-static deformation of the net. The shape of the net is assumed to be constant for each wave period. This is not true in practice since the location of the maximum displacement will be different for the maximum and minimum wave particle velocity when current is present. The location for the maximum amplitude is calculated using the case with the largest force which occurs when the current and fluid particle velocity act in the same direction. The relative velocity between the net and the fluid particle velocity is not considered here or in further derivations.

Using Taylor expansion around $\bar{w} = 0$ the following expression is obtained for the total length,

$$L_{tot} = \alpha L + \frac{1}{2}\frac{\bar{w}^2}{\alpha L} + (1-\alpha)L + \frac{1}{2}\frac{\bar{w}^2}{(1-\alpha)L} \tag{22}$$

For a virtual displacement $\delta\bar{w}$, the virtual elongation, δL_{tot}, is given by

$$\delta L_{tot} = \frac{\bar{w}}{\alpha(1-\alpha)L}\delta\bar{w} \tag{23}$$

When the net is deformed, the axial force, S, will increase due to elongation given by

$$\epsilon = \frac{L_{tot} - L}{L} = \frac{\bar{w}^2}{2L^2\alpha(1-\alpha)} \tag{24}$$

and the total force becomes

$$S_N = S_0 + \frac{EA\bar{w}^2}{2L^2\alpha(1-\alpha)} \tag{25}$$

where S_0 is the pretension.

Inserting S_N into the expression for internal virtual work we get the following expression:

$$\delta W_i = S_N\delta L_{tot} = \frac{S_0\bar{w}}{\alpha(1-\alpha)L}\delta\bar{w} + \frac{EA\bar{w}^3}{2\alpha^2(1-\alpha)^2L^3}\delta\bar{w} \tag{26}$$

The external virtual work is calculated by

$$\delta W_e = \bar{F}_N\delta\bar{w} = \int_{z_b}^{\zeta} f_N\phi\delta\bar{w}dz = -\int_{z_m}^{\zeta} f_N\left(z - z_t\right)\frac{\delta\bar{w}}{\alpha L}dz + \int_{z_b}^{z_m} f_N\left(z - z_b\right)\frac{\delta\bar{w}}{(1-\alpha)L}dz \tag{27}$$

where the force, f_N, ref. Eq. (11), is multiplied with the virtual displacement shape, ϕ, and integrated over the wetted length of the rope. z_t and z_b are the z-coordinates of the top and bottom of the rope, respectively. z_m is the vertical coordinate where the mode shape has its maximum displacement. Eq. (27) is most easily solved using numerical integration.

Equating the internal and the external virtual energy we achieve a 3rd degree equation

$$\delta W_i = \delta W_e \rightarrow \frac{EA\delta\bar{w}}{2L^3\alpha^2(1-\alpha)^2}\bar{w}^3 + \frac{S_0\delta\bar{w}}{\alpha(1-\alpha)L}\bar{w} = \bar{F}_N\delta\bar{w} \tag{28}$$

which can be written on the form:

$$\bar{w}^3 + p\bar{w} + q = 0 \tag{29}$$

with the solution

$$\bar{w} = \sqrt[3]{-\frac{q}{2} - \sqrt{\left(\frac{q}{2}\right)^2 + \left(\frac{p}{3}\right)^3}} + \sqrt[3]{-\frac{q}{2} + \sqrt{\left(\frac{q}{2}\right)^2 + \left(\frac{p}{3}\right)^3}} \tag{30}$$

The axial force in the deformed rope is found by inserting $\bar{w}$ into Eq. (25).

4.5. Total simplified quasi-static response of the rope supporting the net

The total response can be calculated by combining the tangential and normal response of the net. Due to the damping for the case

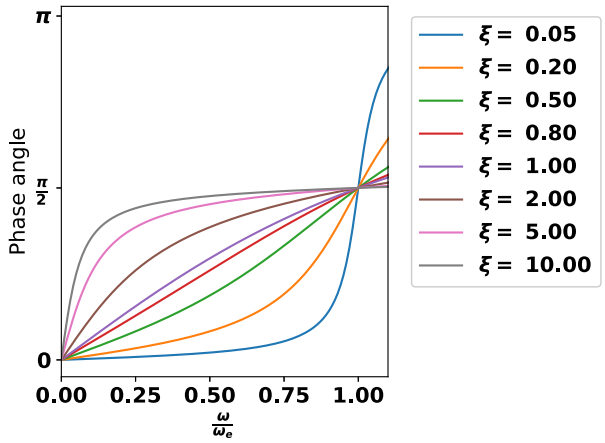

Fig. 6. Phase angle for different critical damping ratios according to linear second order differential equations.

with normal loading, which is not accounted for in the simplified calculations, a phase shift occurs for the axial force compared to the incoming wave. This phase shift does not occur for the tangential force. To achieve a correct response the phase shift for the normal response must be accounted for before summing the two contributions.

The damping can be estimated by considering the maximum excitation force which is drag-dominated.

$$F_{max} = C_N(0)\left(u_c + u_{rel}\right)^2 = C_N(0)\left(u_c^2 + 2u_c u_{rel} + u_{rel}^2\right) \tag{31}$$

Extracting the dynamic part of the equation we get an approximation for the damping:

$$F_{dyn_{max}} = C_N(0)\left(2u_c u_{rel} + u_{rel}^2\right) = \underbrace{C_N(0)\left(2u_c + u_{rel}\right)}_{c}\left(u_w - u_{rope}\right) \tag{32}$$

Considering u_{rel} to be a constant, it is seen the dynamic force consists of an excitation force proportional to u_w and a damping force proportional to u_{rope}.

$$F_{dyn_{max}} = \underbrace{cu_w}_{Excitation} - \underbrace{cu_{rope}}_{Damping} \tag{33}$$

As an upper bound estimate for the damping we may use u_{rel} equal to the wave particle velocity, u_w. The damping constant must be transformed to the system defined by the principle of virtual displacements:

$$\bar{C} = \int_{z_b}^{0} \phi^2 C_N(0)\left(2u_c + u_w\right) dz \tag{34}$$

The phase angle for a linear second order differential equation is used to estimate the phase angle in the current problem. The damping ratio is given by:

$$\xi = \frac{\bar{C}}{2M w_n} \tag{35}$$

where M is the mass and w_n is the natural period. The phase angle is calculated from

$$\theta = \arctan\left(\frac{2\xi\frac{\omega}{\omega_n}}{1 - \frac{\omega^2}{\omega_n^2}}\right) \tag{36}$$

The phase angle for different critical damping ratios is shown in Fig. 6. For the current problem, the frequency ratio is between 0.02 and 0.20 and the estimated critical damping ratio, ξ varies between 0.01 and 12.0.

Once the phase shift is included in the time history for the normal response, the total tension force in the rope is calculated from:

$$S(t) = S_T(t) + S_N(t) \tag{37}$$

4.6. Validity range of the calculation method — normal loading

Two main forces are neglected when the simplified quasi-static method is used; the inertia force and the damping due to the relative velocity. The effect of neglecting these contributions is discussed separately in the following two sections.

4.6.1. Inertia force

If the loading period is much larger than the natural period of the structure, the inertia force can be neglected. The modal period of the assumed deformation modes can be estimated using the equivalent mass and stiffness terms. The stiffness is already calculated. The equivalent mass is derived from the virtual work of the inertia forces

$$\delta W_{inertia} = -\int_{z_b}^{0} \bar{m}\ddot{\bar{w}}\phi\phi\delta\bar{w}\,dz = \int_{z_b}^{0} \phi^2\bar{w}\bar{m}\omega^2\delta\bar{w}\,dz \tag{38}$$

and becomes

$$M = \frac{\bar{m}}{3\alpha^2 L^2}\left[-z_t^3 - \left(z_m - z_t\right)^3\right] + \frac{\bar{m}}{3(1-\alpha)^2 L^2}\left(z_m - z_b\right)^3 \tag{39}$$

To estimate the modal periods we need to assume that the response is harmonic. The linear stiffness in Eq. (28) is used to determine the natural period, $T_0 = 2\pi\sqrt{M/K}$, where $K = \frac{S_0}{\alpha(1-\alpha)L}$.

The unit mass per meter of rope, including the net, is 1.68 kg/m. The density of the rope is very close to 1000 $\frac{kg}{m^3}$ which is close to the density of the sea water. It is reasonable to assume that the density of the net is similar. Since both the net and the rope have a circular cross section, the added mass will be equal to the mass of the displaced volume. The total mass of the rope and net including added mass is therefore estimated to be 2 times the dry mass, i.e. 3.36 kg/m.

With $S_0 = 10^5$ N and $m = 3.36$ kg/m, the modal periods are between 0.26 s and 0.34 s depending on the assumed deformation shape, which depends on the wave period. According to Patel and Park (1991) the natural period for a freely vibrating string is given by

$$T_0 = 2L\sqrt{\frac{\bar{m}}{S}} \tag{40}$$

The natural period using Eq. (40) is 0.38 s. This is in line with the calculations using the principle of virtual displacements.

For our case relevant loads occur for periods greater than 2.0 s. This is more than five times the natural period including added mass. Hence disregarding the inertia effects should be acceptable.

If the pretension is reduced, the natural period will increase. Reducing the pretension with a factor of 10 will increase the natural period including added mass to 0.82–1.08 s. With such a low pretension the inertia may affect the response for periods less than approximately 3.5 s. It should be noted however, that mode shapes for the smallest wave periods have the smallest period. I.e., the net has a modal period equal to 0.82 s for $S_0 = 10^4$ N if the wave period is equal to 2 s.

4.6.2. Relative velocity

The relative velocity is not accounted for in the simplified formulation. In some cases, the velocity of the net may become large and can have significant effect on the axial force in the net. Disregarding the relative velocity will result in a conservative result since the forces acting on the net will be overpredicted. A physical limit is that the motion of the net should be smaller than the motion of the fluid particles. To compare these values a transformation to the coordinate system used for the PVD is needed. The transformation is performed considering the linearized forces shown in Eq. (33).

The virtual work from the linearized damping force is written

$$\delta W_{damping} = c\int_{z_b}^{0} \phi^2\omega w\delta w\,dz \tag{41}$$

and for the linearized excitation force,

$$\delta W_{excitation} = c\int_{z_b}^{0} \phi\omega\zeta e^{kz}\delta w\,dz \tag{42}$$

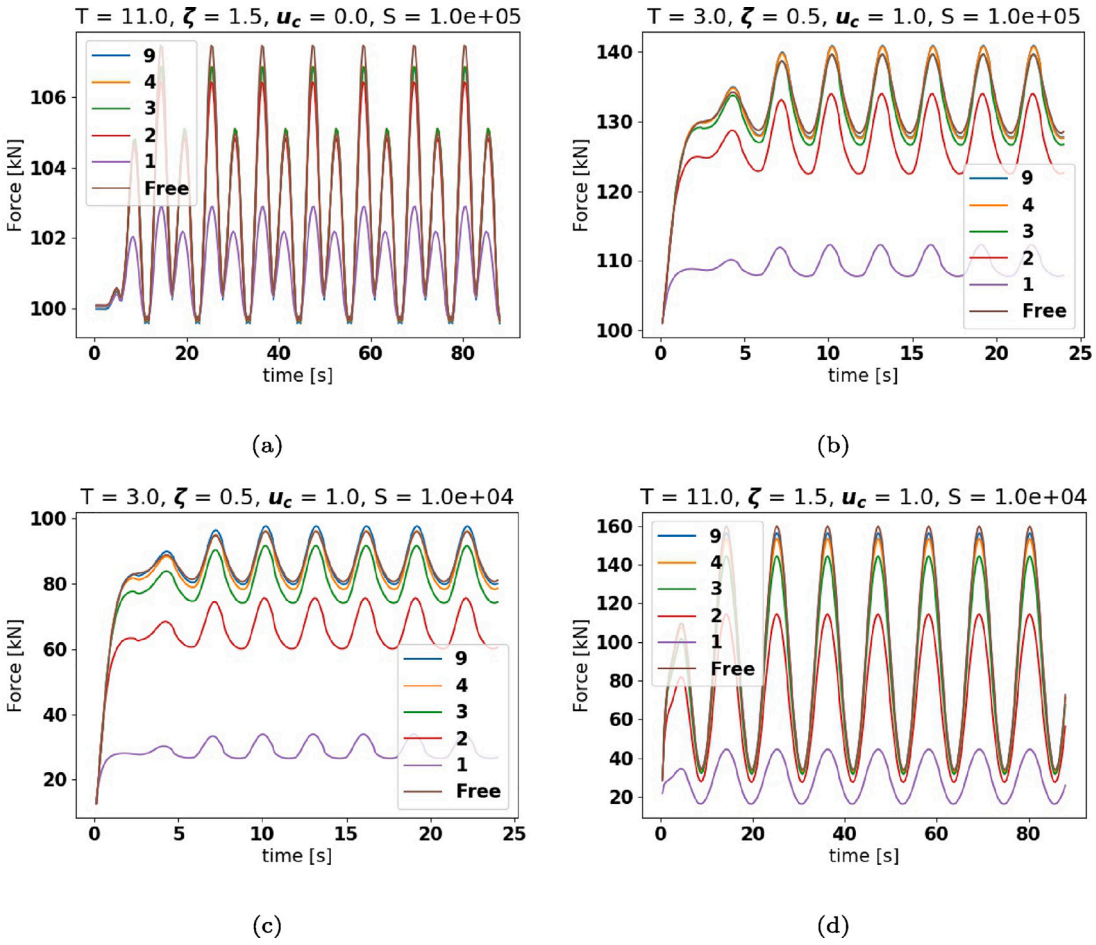

Fig. 7. Time series of the axial force in different lines on the panel for different line numbers.

The ratio suggesting the accuracy of neglecting the relative velocity can be expressed by the ratio of the virtual work for the damping and excitation forces

$$R = \frac{\delta W_{damping}}{\delta W_{excitation}} \tag{43}$$

Although the ratio is a energy or force ratio, it is referred to as a motion ratio since it represents the ratio of the net motion compared to the wave motion. If the ratio is over 1.0, the results will be conservative since it is not physical to have a response greater than the excitation for the present case.

5. Results and numerical simulations

Numerical simulations are preformed to investigate the accuracy of the simplified calculation. First, the set-up of the numerical analyses used to confirm the hypothesis of the single rope compared to panel modeling of the fish net is presented in Section 5.1. This is followed by the description of the numerical model used for the comparison with the simplified calculation method in Section 5.3. The numerical analyses are all performed in SIMA/RIFLEX (Ocean, 2020) which is a non-linear finite element program capable of simulating the time domain response of structures exposed to wave loading.

5.1. Single rope model vs panel model of aquaculture net

The hypothesis of modeling the net response by considering a single rope is checked through numerical simulations. The responses of each rope of a panel, see Fig. 2, is compared to the response of a single free line shown to the right of the panel. Here the viscous force is modeled using the fish net element in RIFLEX which is based on Lølands screen model, (Loland, 1991). In the complete panel model, the load carrying fish net elements are horizontal. In addition to the fish net elements, vertical bar elements are added to the model to represent the vertical stiffness of the supporting rope. The distance between each of the lines is approximately 1.7 m both in the horizontal as well as in the vertical direction.

There are in total 17 lines on the panel shown in Fig. 2. Line no. 1 is next to the steel pipe, and line no. 9 is in the center of the panel. Fig. 7 shows the force time histories of 5 of the lines on the panel in addition to the force history of the free line which is located to the right in Fig. 2. It is seen that the free line conservatively estimates the axial force for all lines. For line 1 and 2 the results are overly conservative, but for the rest the force estimate is reasonable or slightly conservative. Based on the results in Fig. 7 it is concluded that it is relevant to estimate the response using a single rope since it provides a reliable estimate for 13 out of the 17 lines.

5.2. Validation of assumed displacement shape

The quasi-static net shape from Eq. (19) is compared to the dynamic shape of the rope from non-linear analyses in SIMA/RIFLEX in regular waves in Fig. 8 . In general it is seen that the largest deviation between actual and estimated shape occurs for steep waves, low pretension and for low periods. The assumed shape is generally less accurate when the deformation is large compared to the wave amplitude.

For a pretension equal to 10^5 N, Fig. 8 shows that the quasi-static shape is almost identical to the simulated shape for all periods. For the softest case with a pretension of only 10^4 N, it is seen that there is a

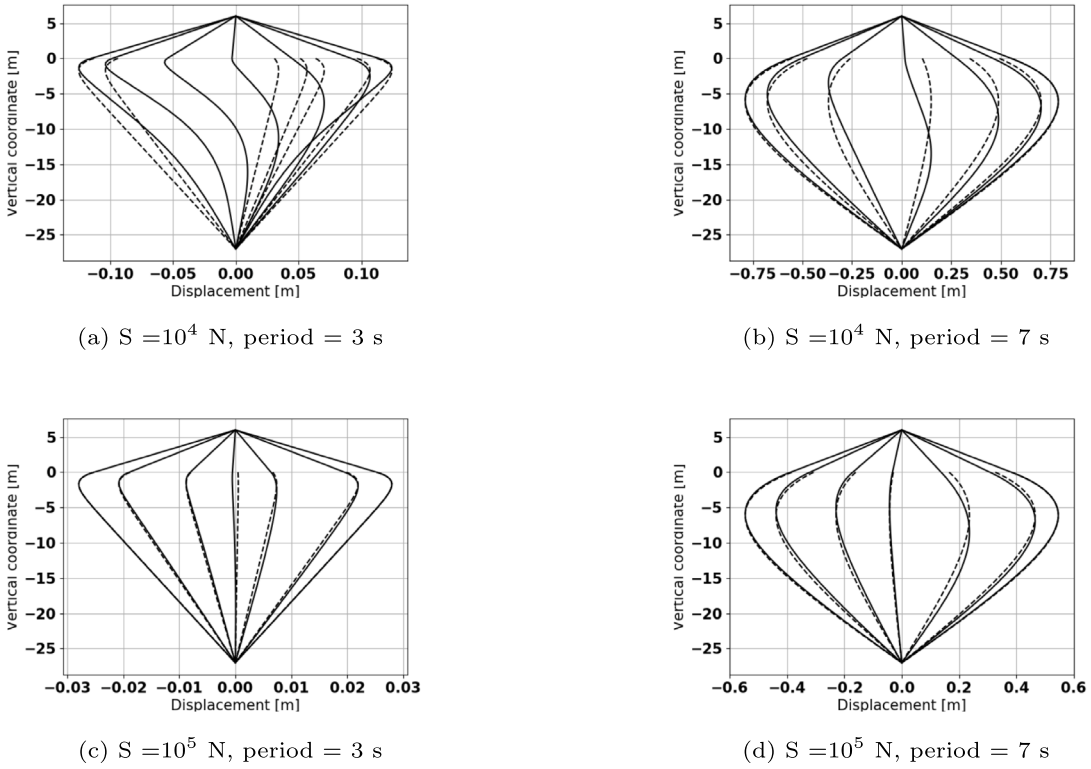

Fig. 8. Comparison of deformation shape. Dashed line is semi-empirical solution, solid line is from RIFLEX. Results from both methods are scaled to identical amplitudes.

significant deviation for the smaller periods. The shape at maximum displacement is however well estimated for all cases.

5.3. Analyses in regular waves and current

Numerical simulations are performed in RIFLEX for comparison with the simplified calculations. The rope supporting the fish net is modeled in a simplified manner as described in Section 2. i.e. as a single line pinned at both ends. The loads acting on the rope are calculated by the Fish net elements which uses Lølands screen model up to the exact free surface. The loads from the fish net are lumped to the rope similar as for the simplified model. The rope is modeled with 100 bar elements. The mass including added mass is set equal to 3.36 kg/m. Deep water conditions are assumed. To ensure that the results are representative for the steady state case, the analysis is run until convergence is achieved, which is for all cases was less than 8 wave periods. All analyses are therefore run for 8 wave periods.

Due to numerical issues a stiffness proportional damping factor on the material stiffness equal to 0.05 was introduced. Without damping the analysis was unstable in some cases.

The stiffness of the rope is defined using a linear force elongation curve. The force at zero elongation is equal to the pretension.

A series of numerical simulations are performed for different combinations of wave period and wave height for different current velocities. The periods and wave amplitudes are listed in Table 2 and the current velocities in Table 3. All wave conditions in Table 2 are combined with each current in Table 3.

To test the limits of the simplified method, a case with a reduced pretension equal to 10^4 N is analyzed in addition to the realistic case with a pretension equal to 10^5 N. The analyses with reduced pretension is used to investigate the accuracy of the simplified method when dynamics are of greater importance.

Time histories of the axial force are compared in Fig. 9 for a pretension equal to 10^5 N and Fig. 10 for a pretension equal to 10^4 N. It is seen that the time history is well predicted when using the simplified

Table 2
Wave amplitudes and heights of regular waves.

Case	Wave amplitude[m]	Period [s]
1	0.25	2
2	0.25	3
3	0.25	4.5
4	0.25	6.5
5	0.25	9
6	0.25	11.5
7	0.5	3
8	0.5	4.5
9	0.5	6.5
10	0.5	9
11	0.75	3.5
12	0.75	6
13	1.0	6
14	1.5	6

Table 3
Current velocities.

Current velocity [m/s]			
0.0	0.1	0.5	1.0

calculation when the pretension is 10^5. When the pretension is reduced to 10^4 N it is observed that the simplified method overestimates the axial force. The accuracy is considered acceptable in the initial design stage in view of the significantly reduced computation time from 55 min in the numerical simulations to seconds with the simplified method.

The results from the numerical simulations as well as from the simplified calculation are presented in Fig. 11, for rope fatigue and Fig. 12, for fatigue of a steel connection point. The fatigue life is normalized to 1.0 for each sea condition when the current velocity is equal to zero. The damages from the different sea states are thus not comparable. The results from the numerical simulations are shown as

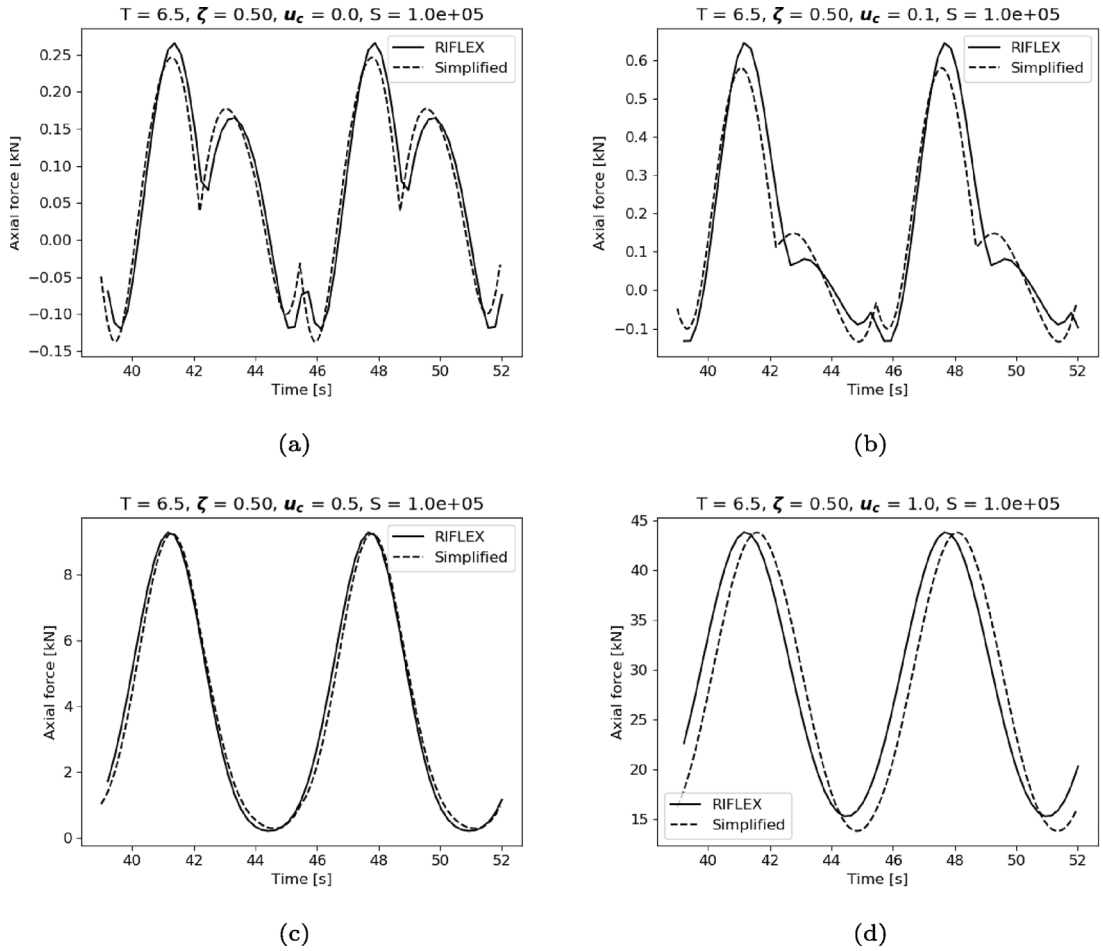

Fig. 9. Time series of the axial force in different current velocities for a pretension equal to 10^5 N.

solid lines and the results from the simplified calculations are shown as solid dots.

Figs. 11 and 12 shows that the accuracy of the simplified calculations is reasonable for many cases. There are however several cases where the error is quite large. This is especially true when the pretension is reduced to 10^4. The actual pretension in the ropes on the OF1 is close to 10^5 N. Hence, for realistic cases, the accuracy of the results should be in line with the results for S = 10^5 N presented herein. The reduction of the pretension to S = 10^4 N is performed to show that the method is less accurate for some cases. For all the cases we can see that neglecting the effect of current would lead to a significant overestimation of the fatigue life.

The comparisons of the time histories in Figs. 9 and 10 and the comparison of the estimated fatigue life in Figs. 11 and 12 show both that the simplified method is in good agreement with the numerical simulations. The accuracy of the simple method is the largest for the cases where the pretension is 10^5 N because the velocity of the rope, which is not included in the simplified method is small.

The results of the fatigue life calculations displayed in Figs. 11 and 12 show that the current velocity has a major affect on the fatigue life. For the rope the current increases the total load which gives a reduced fatigue life due to an increase in the total tension level. For the steel connection the fatigue life is reduced due to an increase of the dynamic tension from the cross coupling of the wave and current in the non-linear load formulation. The effect is much greater for the fatigue life of the steel connection than it is for the "fatigue" of the rope which is determined by creep. The reason is that the creep model uses the total stress level as input whereas the cyclic fatigue calculations uses the stress range as input. The current affects the stress range much more than the total stress level since the system is under pretension. It is seen that the reduction of the fatigue life from the current for the steel connection is the greatest for a large pretension. For the fatigue life of the rope however, the reduction due to current becomes much larger when the pretension is decreased. The results show that the influence the current has on the fatigue life varies depending on the fatigue model as well as the stiffness of the system. It is therefore difficult to generalize how much current affects the structure.

6. Discussion

6.1. Basic assumptions

The simplified computation model is based on some idealized assumptions which are not always in line with reality. In the following sections some of the assumptions are discussed.

6.1.1. Single rope model

The hypothesis to model the response of the panel with a single rope is verified according to the results presented in Fig. 7. This type of simplification is commonly used in engineering for both stress as well as buckling analyses of stiffened panels with great success. The results from the free rope analyses are conservative for all the ropes in the panel since the calculated force for each of the ropes in the panel is either smaller or equal to the force in the free rope. This is similar to that of the single stiffener including plate flange compared to a stiffened panel. Hence, the simplification can be used for design cases. It should be noted that only waves propagating normally to the net are considered in the present paper.

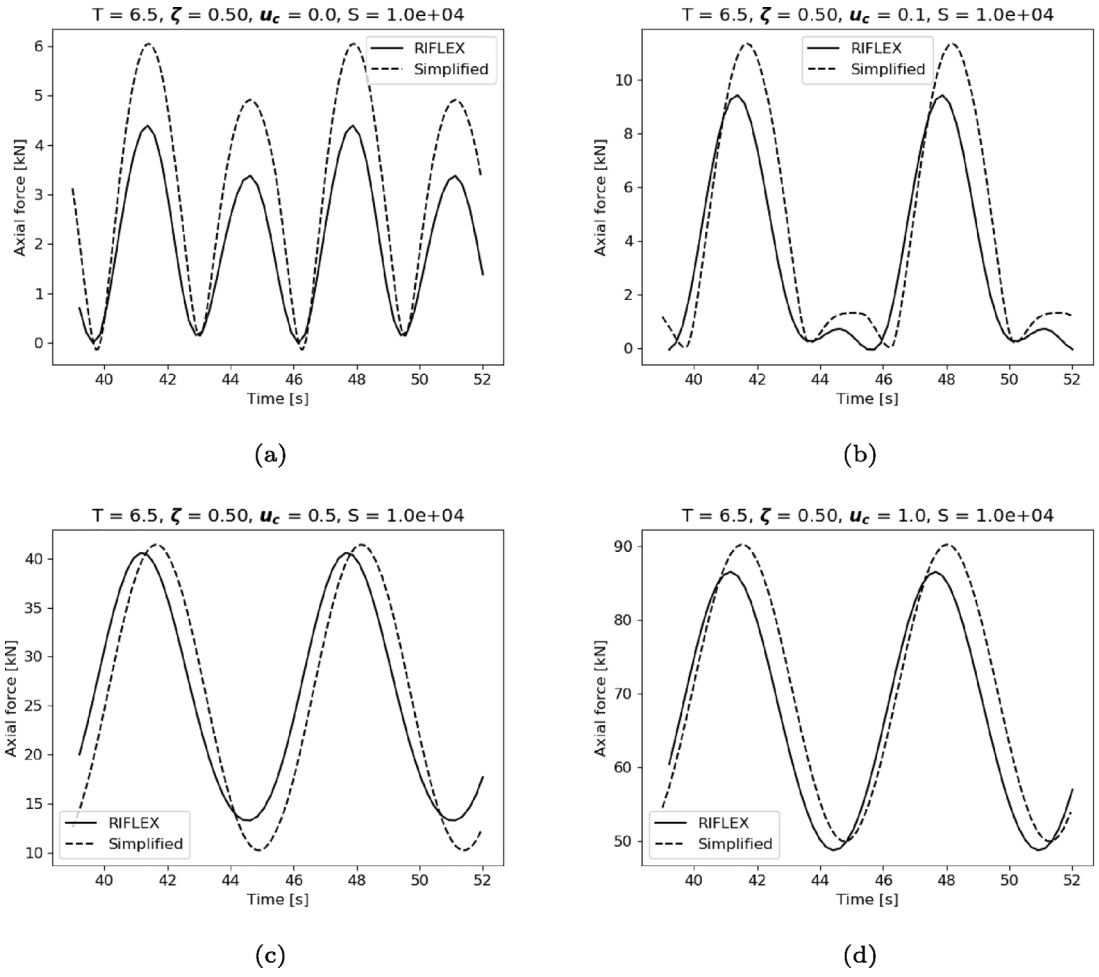

Fig. 10. Time series of the axial force in different current velocities for a pretension equal to 10^4 N.

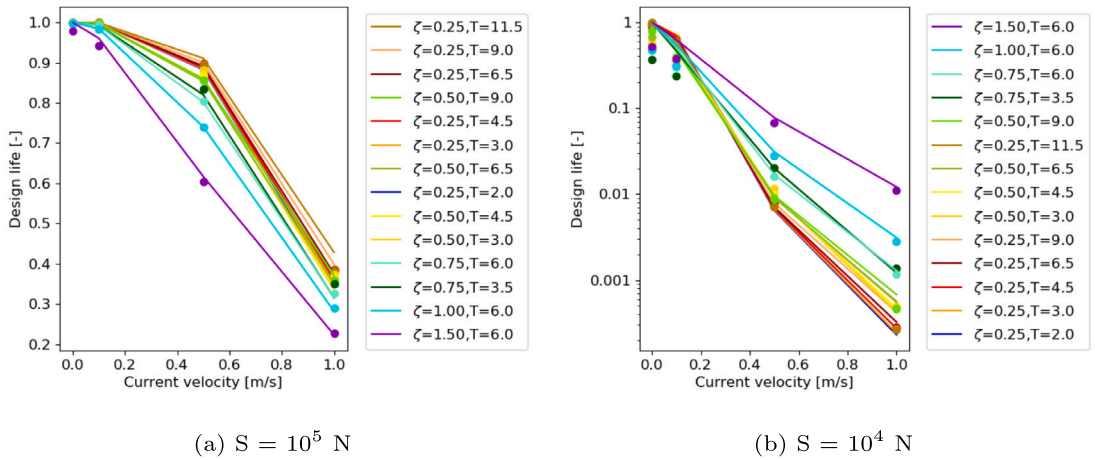

Fig. 11. Change in fatigue life as a function of current velocity for different wave periods and wave heights. Solid lines are numerical analyses. Dots are simple hand calculations based on PVD. Fatigue calculations based on creep.

6.1.2. Splitting of response — normal and tangential

The viscous loads are in the simplified calculations method divided into a normal contribution and a tangential contribution and the responses are calculated separately before they are added together. This type of splitting is commonly used in linear analysis, but is not generally possible for non-linear analyses. The splitting is considered admissible even though both the loading and the response is non-linear since the responses have a very small effect on each other. The tangential load changes the axial force in the rope, but the change is small compared to the pretension and can therefore be disregarded when calculating the response from the normal load. Also, the horizontal displacement caused by the normal load is small compared to the length of the rope and has therefore only a minor effect on the vertical stiffness which is important when calculating the axial force from the tangential load.

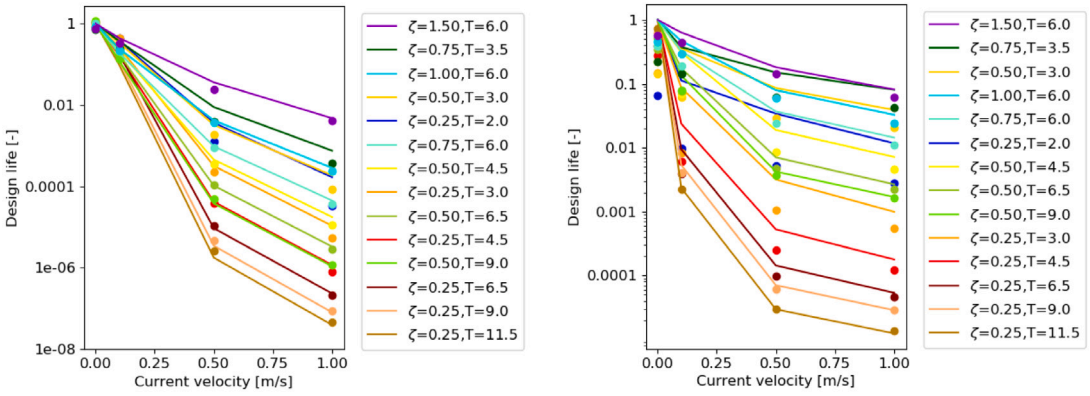

(a) S = 10^5 N (b) S = 10^4 N

Fig. 12. Change in fatigue life as a function of current velocity for different wave periods and wave heights. Solid lines are numerical analyses. Dots are simple hand calculations based on PVD. Fatigue for steel detail with m = 3.0.

Table 4
Damage and force errors for extreme cases from Fig. 14.

Case	$\frac{Life_{simple}}{Life_{numerical}}$	$\frac{D_{simple}}{D_{numerical}}$	$\frac{F_{simple}}{F_{numerical}}$
S=10^4 N	0.28	3.6	1.53
S=10^5 N	2.00	0.50	0.79
S=10^5 N	1.50	0.67	0.88

Before adding the responses together it is essential that the phase shift of the response from the normal load is accounted for. In the present method an upper limit of the damping is used when the phase shift is estimated based on linear second order differential equations. The effects of using a different estimate of damping is not investigated since the predicted phase shift is in line with the numerical simulations.

6.1.3. Mode shape for normal loading

The assumed deformation shape is a simplification of the actual deformation shape and introduces inaccuracies in the estimation of the axial force. For cases with zero current and for cases with large current velocities compared to the wave particle velocity, the assumed deformation shape is reasonable. See Figs. 13 (c) and (d) for a comparison of deformation shape for cases with large current velocities. For intermediate current velocities, the resultant velocity may change sign when the current and wave acts against each other at a certain depth. The quasi-static shape and also the dynamic shape of the net will then be a deformed "S" as seen in Fig. 13(a) for which the assumed triangular shape is not good. Nevertheless, the accuracy of the fatigue life estimation is reasonable for these cases. The reason may be that the "S" shape and hence the inaccurate mode shape can only occur for negative amplitudes. The assumption of the triangular deformation shape is reasonable for the positive amplitudes as seen in Fig. 13(b), where the current and wave particle velocity act in the same direction. For fatigue calculations the largest amplitudes in the time series contribute the most and the accuracy of the estimated fatigue damage remains high even though the mode shape is not good for the minimum amplitude.

6.2. Computation time

The computation time is greatly reduced with the simplified calculation method compared to the numerical analyses. A series of 56 numerical simulations are performed using RIFLEX, taking a total 55 min to complete. The simplified calculation method performs the same calculations in 10.3 s. This is only 0.3% of the time needed to perform the analyses in RIFLEX. In a design process many more design iterations can be performed using the simplified method which may result in a better design. The main reason for the huge improvement in computation time is due to the very small time step needed in the numerical simulations to keep the analyses from failing.

6.3. Limitations of the simplified calculation method

The main error in the simple calculation method is that the relative velocity is not accounted for as described in Section 4.6.2. Fig. 14 shows the ratio of the fatigue life for the steel connection calculated using the simplified method divided by the numerical fatigue life estimation on the y-axis. On the x-axis, is the motion ratio, which is defined as the rope motion amplitude divided by the fluid motion amplitude calculated according to Section 4.6.2. It is seen that the fatigue life ratio decreases for increasing motion ratio, i.e. the degree of fatigue life underestimation increases with an increasing motion ratio. The hypothesis that the results are conservative for a motion ratio greater then 1.0 is in line with the results in Fig. 14.

It is seen that the motion ratio is below 1.0 for most cases when the pretension is 10^5 N. There are only 8 cases where the motion ratio is above 1.0 all with small wave periods ($< 4s$) and large current velocities (0.5 & 1.0 m/s). For the softer case when the pretension is 10^4 N there are many more cases above the assumed limit of 1.0. Again these are for the cases with small wave periods. All cases have periods equal to or below 4.5 s. For the case with an artificially low pretension, the largest damage ratio with a motion ratio less than 1.0 is 3.6. Hence, the estimated lifetime is only 28% of the actual lifetime calculated using NLFEA.

There are some cases in Fig. 14 that have non-conservative results. See the dashed circle. For these cases the inaccuracy is due to the calculation method which has trouble with small waves combined with intermediate current velocities. In most cases these sea states will have very little contribution to the total damage due to the small wave amplitude. For the most extreme case, the fatigue life ratio is overestimated by 100%. However the actual fatigue damage from sea states with such a small wave amplitude is small and therefore generally not of importance. Not considering the sea states in the dashed circle, the error in the fatigue life overestimation is smaller than 50%.

The fatigue lives shown in Fig. 14 are calculated using an SN-curve with $m = 3$. If it is assumed that the fatigue damage is from a constant amplitude load, the error in force is found using:

$$\frac{F_{simple}}{F_{numerical}} = \left(\frac{D_{simple}}{D_{numerical}}\right)^{1/m} \tag{44}$$

Table 4 summarizes the magnitudes of the errors discussed in the forgoing paragraphs. The error in force for the low pretension case is

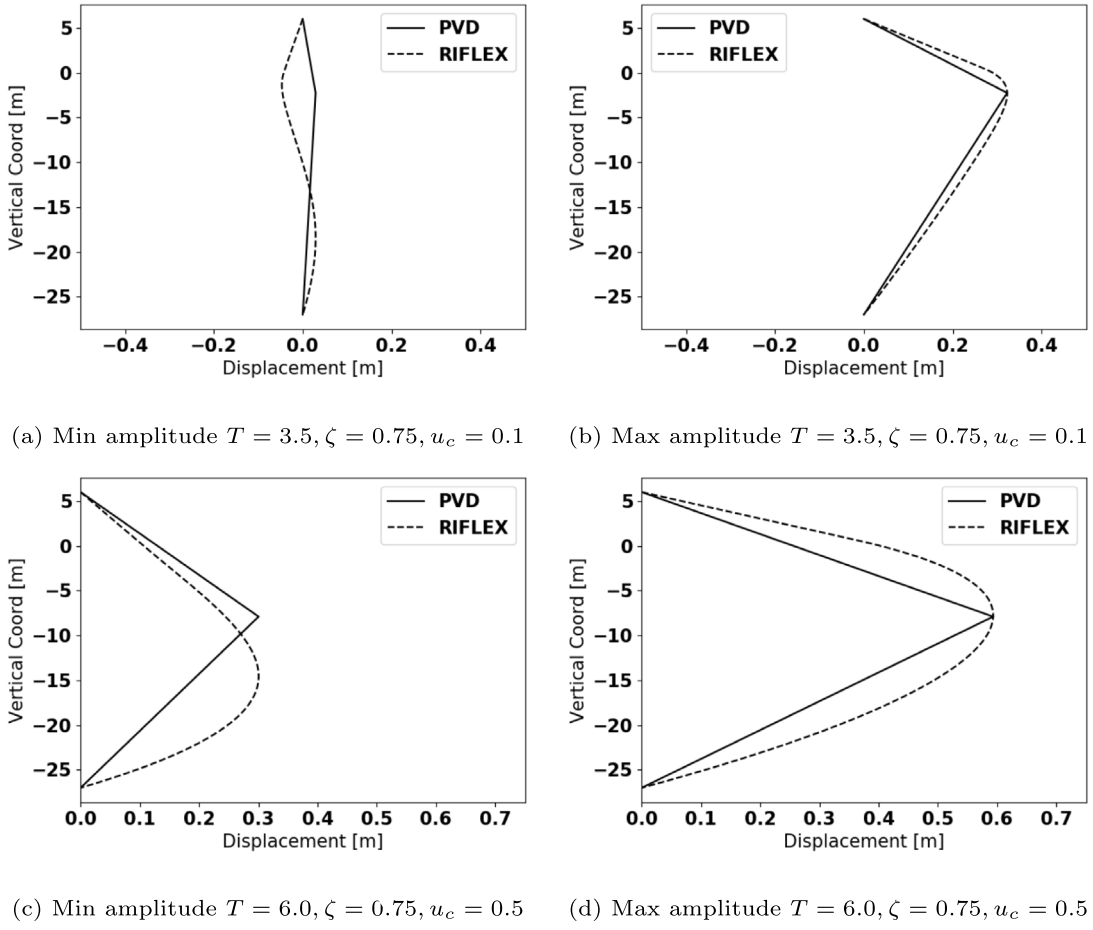

(a) Min amplitude $T = 3.5, \zeta = 0.75, u_c = 0.1$ (b) Max amplitude $T = 3.5, \zeta = 0.75, u_c = 0.1$

(c) Min amplitude $T = 6.0, \zeta = 0.75, u_c = 0.5$ (d) Max amplitude $T = 6.0, \zeta = 0.75, u_c = 0.5$

Fig. 13. Comparison of assumed deformation shape, solid, to RIFLEX results, Dashed. Results are scaled to equal amplitude.

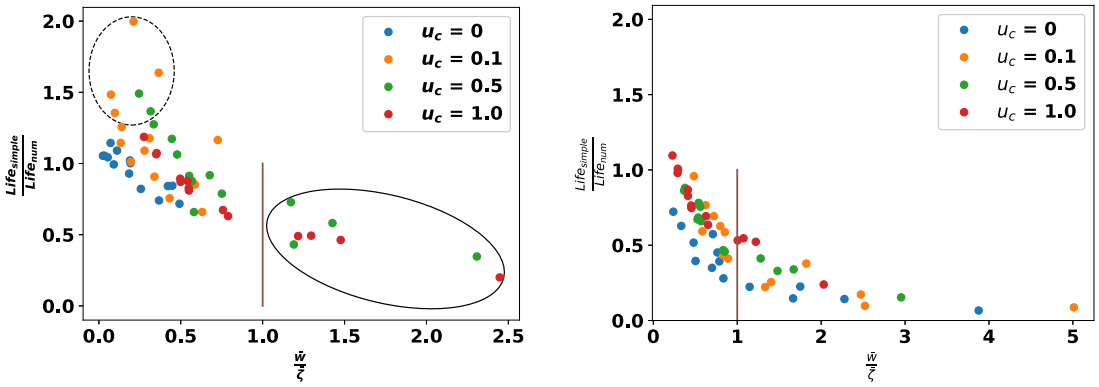

(a) S = 10^5 N (b) S = 10^4 N

Fig. 14. Scatter of the fatigue life for the steel connection from the simplified method divided by the numerical fatigue life versus the relative motion force ratio from Eq. (43). (a) Solid circle shows cases with wave periods less than 4.0 s. Dashed circle shows cases with wave amplitude equal to 0.25 m.

up to a 53% overestimation. For the realistic case where the pretension is 10^5 N, the underestimation of the force will generally be smaller than 12%. For the worst case in Fig. 14 it is seen that the force was underestimated by 21%.

With such a good accuracy the simplified method can be used in a design phase to calculate initial estimates. The motion ratio can be used to give an indication regarding the conservatism of the estimate. In addition, the method is useful to verify the results of complex simulations according to Norsok et al. (2021). Norsok et al. (2021) is not a requirement for aquaculture structures, but it represents good practice.

7. Conclusion

In the present paper a simplified model is presented to estimate the axial forces in the fish net supporting ropes of an offshore fish farm under waves and current. Quasi-static mode shapes are adopted

considering the large rope stiffness and stiffness dominated rope response. The resulting axial forces are used further for creep and fatigue assessment of the rope and the steel connection. In the proposed model, the viscous load is divided into a tangential contribution and a normal contribution. The response to the loads are calculated individually and summed together to achieve the time history for the axial force in the rope.

The accuracy of the simplified method is evaluated by comparing calculated fatigue damage to that obtained with numerical simulations with the RIFLEX software. Good agreement is found for ropes with a typical pretension, where the motion of the rope is of little importance. With small pretension the motions of the rope becomes significant and affects the fatigue damage. The simplified method is mostly conservative and may still be useful in early design. Based on the results herein, the error of fatigue life estimation, is generally less than 50% on the non-conservative side. This is equivalent to 12% underestimation of the dynamic force. A parameter, "motion ratio" is proposed to give an indication regarding the conservatism in the simplified method.

When the following conditions are met, it is expected that the simplified method will produce results that are of acceptable for initial design estimations as well as for analysis verification analogous to the requirements in NORSOK N-001, (Norsok et al., 2021).

- Wave and/or current like loading
- Rope fixed at top and bottom
- Natural period of rope is small compared to the loading period
- The velocity of the rope is small compared to the fluid particle velocity to avoid overly conservative results

The study shows that current has a strong effect on the fatigue life of both the rope as well as the connection point fabricated in steel. Neglecting the current will in many cases produce unreliable and non-conservative estimates of the fatigue life. The reduction in fatigue life due to current is the largest for the connection point with large pretension. Conversely, for the rope the change in fatigue life is the greatest when the pretension is the lowest.

The proposed method is extremely efficient compared to current calculation methods based on NLFEA. For a given set of cases the simplified method used 10.3 s to complete the calculation while the accurate NLFEA used 55 min. The simplified method is therefore highly suitable for design when quick, conservative estimates are desired.

CRediT authorship contribution statement

Martin Slagstad: Simplified method, Performed numerical simulations, Writing – original draft. **Zhaolong Yu:** Academic advisors, Reviewed & commented paper. **Jørgen Amdahl:** Academic advisors, Reviewed & commented paper.

Declaration of competing interest

The authors declare that they have no known competing financial interests or personal relationships that could have appeared to influence the work reported in this paper.

Data availability

No data was used for the research described in the article.

Acknowledgments

This work was supported by the Research Council of Norway through the Centre of Excellence funding scheme, NTNU AMOS, project number 223254.

References

Bore, P.T., Amdahl, J., 2017. Determination of environmental conditions relevant for hte ultimate limit state at an exposed aquaculture location. pp. 1–14.
Bore, P.T., Amdahl, J., Kristiansen, D., 2017. Modelling of hydrodynamic loads on aquaculture net cages by a modified morison model. In: 7th International Conference on Computational Methods in Marine Engineering, MARINE 2017. 2017-May, pp. 647–662.
DNV, 2014. Fatigue design of offshore steel structures, DNVGL-RP-0005.
Dong, G.H., Tang, M.F., Xu, T.J., Bi, C.W., Guo, W.J., 2019. Experimental analysis of the hydrodynamic force on the net panel in wave. Appl. Ocean Res. 87 (January), 233–246. http://dx.doi.org/10.1016/j.apor.2019.04.005.
DSM, 2008. Dyneema high-strength, high-modulus polyethylene fiber. pp. 1–4, URL https://www.dyneema.com.
Faltinsen, O.M., Timokha, A.N., 2009. Sloshing. Cambridge University Press.
Føre, H.M., Dahle, S.W., Gaarder, R.H., 2019. Tensile strength of Nylon netting subjected to various concentrations of disinfecting chemicals. J. Offshore Mech. Arct. Eng. 141 (1), 1–8. http://dx.doi.org/10.1115/1.4040562.
Humeau, C., Davies, P., Smeets, P., Engels, T.A., Govaert, L.E., Vlasblom, M., Jacquemin, F., 2018. Tension fatigue failure prediction for HMPE fibre ropes. Polym. Test. 65 (October 2017), 497–504. http://dx.doi.org/10.1016/j.polymertesting.2017.12.014.
Jensen, Dempster, T., Thorstad, E.B., Uglem, I., Fredheim, A., 2010. Escapes of fishes from Norwegian sea-cage aquaculture: Causes, consequences and prevention. Aquac. Environ. Interact. 1 (1), 71–83. http://dx.doi.org/10.3354/aei00008.
Jusoh, I., Munshi, S.M., 2018. Effects of current velocity and profile on loading of off shore jacket structure. Int. J. Eng. Trends Technol. 59 (2), 108–112. http://dx.doi.org/10.14445/22315381/ijett-v59p218.
Kristiansen, T., Faltinsen, O.M., 2012. Modelling of current loads on aquaculture net cages. J. Fluids Struct. 34, 218–235. http://dx.doi.org/10.1016/j.jfluidstructs.2012.04.001.
Kristiansen, T., Faltinsen, O.M., 2015. Experimental and numerical study of an aquaculture net cage with floater in waves and current. J. Fluids Struct. 54, 1–26. http://dx.doi.org/10.1016/j.jfluidstructs.2014.08.015.
Lader, P., Jensen, A., Sveen, J.K., Fredheim, A., Enerhaug, B., Fredriksson, D., 2007. Experimental investigation of wave forces on net structures. Appl. Ocean Res. 29 (3), 112–127. http://dx.doi.org/10.1016/j.apor.2007.10.003.
Loland, G., 1991. Current forces on and flow through fish by geir loland division of marine hydrodynamics the norwegian institute of technology.
Mjåtveit, M.A., Cheng, H., Ong, M.C., Lee, J., 2021. Comparative study of circular and square gravity-based fish cages with different dimensions under pure current conditions. Aquac. Eng. 96 (December 2021), 102223. http://dx.doi.org/10.1016/j.aquaeng.2021.102223.
Moe Føre, H., Christian, E.P., Norvik, C., Lader, P., 2020. Hydrodynamic Loads on net panels with different solidities. In: 39th International Conference on Ocean, Offshore and Arctic Engineering, OMAE2020. 2020.
Moe-Føre, H., Endresen, P.C., Bjelland, H.V., 2021. Load coefficients and dimensions of raschel knitted netting materials. pp. 1–10.
Moe-Føre, H., Lader, P.F., Lien, E., Hopperstad, O.S., 2016. Structural response of high solidity net cage models in uniform flow. J. Fluids Struct. 65 (7465), 180–195. http://dx.doi.org/10.1016/j.jfluidstructs.2016.05.013.
Mohapatra, S.C., Bernardo, T.A., Soares, C.G., 2021. Dynamic wave induced loads on a moored flexible cylindrical net cage with analytical and numerical model simulations. Appl. Ocean Res. 110 (February), 102591. http://dx.doi.org/10.1016/j.apor.2021.102591.
Norsok, T., Oil, T.N., Federation, T., Industry, N., 2021. Norsok Standard. pp. 1–48.
Ocean, S., 2020. RIFLEX 4.18.1 User Guide.
Patel, M.H., Park, H.I., 1991. Dynamics of tension leg platform tethers at low tension. Part I - Mathieu stability at large parameters. Mar. Struct. 4 (3), 257–273. http://dx.doi.org/10.1016/0951-8339(91)90004-U.
Soares, S., Green, D.M., Turnbull, J.F., Crumlish, M., Murray, A.G., 2011. A baseline method for benchmarking mortality losses in Atlantic salmon (Salmo salar) production. Aquaculture 314 (1–4), 7–12. http://dx.doi.org/10.1016/j.aquaculture.2011.01.029.
Standards Norway, 2009. Norwegian Standard NS 9415.E:2009 Marine fish farms - Requirements for site survey, risk analyses, design, dimensioning, production, installation and operation. URL http://www.standard.no/en/Nyheter-og-produkter/Campaigns/Fiskeri-landbruk-og-mat/Marine-fish-farms/.
Vlasblom, M., Bosman, R., Canedo, J., Davies, P., 2019. Designing HMPE fiber ropes on durability. In: OCEANS 2019 - Marseille, OCEANS Marseille 2019. 2019-June, http://dx.doi.org/10.1109/OCEANSE.2019.8867099.
Vlasblom, M., Engels, T., Humeau, C., 2017. Tension endurance of HMPE fiber ropes. In: OCEANS 2017 - Aberdeen. 2017-October, pp. 1–8. http://dx.doi.org/10.1109/OCEANSE.2017.8084939.
Wang, S., Shen, W., Guo, J., Yuan, T., Qiu, Y., Tao, Q., 2020. Engineering prediction of fatigue strength for copper alloy netting structure by experimental method. Aquac. Eng. 90 (May), 102087. http://dx.doi.org/10.1016/j.aquaeng.2020.102087.
Zhao, Y.P., Li, Y.C., Dong, G.H., Gui, F.K., Wu, H., 2008. An experimental and numerical study of hydrodynamic characteristics of submerged flexible plane nets in waves. Aquac. Eng. 38 (1), 16–25. http://dx.doi.org/10.1016/j.aquaeng.2007.10.004.